Available online at www.sciencedirect.com
SCIENCE DIRECT®
Nuclear Instruments and Methods in Physics Research A 556 (2006) 119–133
NUCLEAR INSTRUMENTS & METHODS IN PHYSICS RESEARCH Section A
www.elsevier.com/locate/nima

The MINOS calibration detector

P. Adamson[a], G. Crone[a], L. Jenner[a], R. Nichol[a], R. Saakyan[a], C. Smith[a], J. Thomas[a], M. Kordosky[b,*], K. Lang[b], P. Vahle[b], A. Belias[c], T. Nicholls[c], G. Pearce[c], D. Petyt[c], M. Barker[d], A. Cabrera[d], J. Hartnell[d], P.S. Miyagawa[d], N. Tagg[d], A. Weber[d], E. Falk Harris[e], P.G. Harris[e], R. Morse[e], P. Symes[e], D. Michael[f], P.J. Litchfield[g], R. Lee[h], S. Boyd[i]

[a]*University College London, Gower Street, London WC1E 6BT, UK*
[b]*University of Texas, Austin, Texas 78712, USA*
[c]*Rutherford Appleton Laboratory, Chilton, Didcot, Oxon OX11OQX, UK*
[d]*Oxford University, Keble Road, Oxford OX1 3RH, UK*
[e]*University of Sussex, Falmer, Brighton BN1 9QH, UK*
[f]*California Institute of Technology, Pasadena, CA 91125, USA*
[g]*University of Minnesota, Minneapolis, Minnesota 55455, USA*
[h]*Harvard University, Cambridge, MA 02138, USA*
[i]*University of Pittsburgh, Pittsburgh, PA 15260, USA*

Received 9 September 2005; accepted 16 October 2005
Available online 18 November 2005

Abstract

This paper describes the MINOS calibration detector (CalDet) and the procedure used to calibrate it. The CalDet, a scaled-down but functionally equivalent model of the MINOS Far and Near detectors, was exposed to test beams in the CERN PS East Area during 2001–2003 to establish the response of the MINOS calorimeters to hadrons, electrons and muons in the range 0.2–10 GeV/c. The CalDet measurements are used to fix the energy scale and constrain Monte Carlo simulations of MINOS.

PACS: 29.40.Vj; 29.40.Gx; 29.40.Mc; 85.60.Ha

Keywords: Neutrino detector calibration; Iron-scintillator sampling calorimeter; Test beam measurements

1. Introduction

The Main Injector Neutrino Oscillation Search (MINOS) is a long baseline, two-detector neutrino oscillation experiment that will use a muon neutrino beam produced by the Neutrinos at the Main Injector (NuMI) facility at Fermi National Accelerator Laboratory (FNAL) [1,2]. The measurement will be conducted by two functionally identical detectors, located at two sites, the Near Detector (ND) at FNAL and the Far Detector (FD) in the Soudan Underground Laboratory in Minnesota. The NuMI beamline [3] and the 735 km long baseline will allow exploration of the Δm^2_{23} and $\sin^2(2\theta_{23})$ mixing parameters studied previously with atmospheric neutrinos [4] and by the K2K experiment [5]. For $\nu_\mu \rightarrow \nu_e$ transitions, MINOS will probe neutrino mixing parameters beyond the current limits of the CHOOZ experiment [6].

MINOS endeavors, in the case of oscillations, to measure Δm^2_{23} and $\sin^2(2\theta_{23})$ with an accuracy of better than 10%. To reach that level of precision, the experiment has established a calibration target of $<5\%$ for the uncertainty in the absolute energy scale and a second target of $<2\%$ for the uncertainty in relative calibration between the Near and Far detectors. Since the Near and Far detectors are large and have been constructed underground, a dedicated Calibration Detector (CalDet) was built to establish the energy scale and develop the calibration technique.

*Corresponding author. Tel.: +44 20 7679 3775; fax: +44 20 7679 7145.
E-mail addresses: kordosky@fnal.gov, kordosky@hep.ucl.ac.uk (M. Kordosky).

0168-9002/$ - see front matter © 2005 Elsevier B.V. All rights reserved.
doi:10.1016/j.nima.2005.10.072

The primary goal of the CalDet is to determine the calorimetric response to electrons, hadrons and muons as a function of particle energy. Furthermore CalDet is used to demonstrate that the Near and Far detectors can be precisely calibrated relative to each other. In addition to providing the calibration of the MINOS detectors, the CalDet measurements are used to tune the Monte Carlo detector simulation. Moreover, the study of electromagnetic and hadronic event topology provides essential input into the pattern recognition algorithms used to analyze the neutrino data.

This paper describes measurements made with the CalDet in a series of runs in the CERN Proton Synchrotron T7 and T11 test beams. Specifically, it focuses on the steps necessary to intra-calibrate the MINOS detectors. The CalDets response to electrons, hadrons and muons will be the subject of subsequent papers.

2. The MINOS calibration detector

2.1. Calorimeter composition

The three MINOS detectors are tracking-sampling calorimeters. The active medium comprises 4.1 cm-wide, 1.0 cm-thick plastic scintillator strips arranged side by side into planes. Each scintillator plane is encased within aluminum sheets to form a light-tight module and then mounted on a steel absorber plate. The detectors are composed of a series of these steel-scintillator planes hung vertically at a 5.94 cm pitch with successive planes rotated by 90° to measure the three dimensional event topology. The CalDet (a sub-section of which is shown in Fig. 1) consisted of 60 planes with 24 100 cm-long strips in each. Wavelength-shifting (WLS) and clear optical fibers transport scintillation light from each strip to Hamamatsu multi-anode photomultiplier tubes [7] which reside in light-tight boxes alongside the detector.

Each scintillator strip is made of Dow STYRON 664 polystyrene doped with the fluors PPO and POPOP (1% and 0.03% by weight) [8]. The strips were produced in an extrusion process during which a 2.0 mm-wide, 2.0 mm-deep groove was driven along each strip. The entire strip, apart from the groove, was co-extruded with a 0.25 mm-thick reflective layer made of polystyrene doped with 15% TiO_2 by weight. Scintillation light is collected by a 1.2 mm-diameter WLS fiber [9] that was glued into the groove with optical epoxy [10]. The WLS fiber conducts the light to an optical connector located on the edge of the scintillator layer where it is transferred to a clear polystyrene fiber and routed to the photomultipliers.

The CalDet steel plates were 1 m × 1 m square and 2.50 cm-thick. The detector was unmagnetized, in contrast

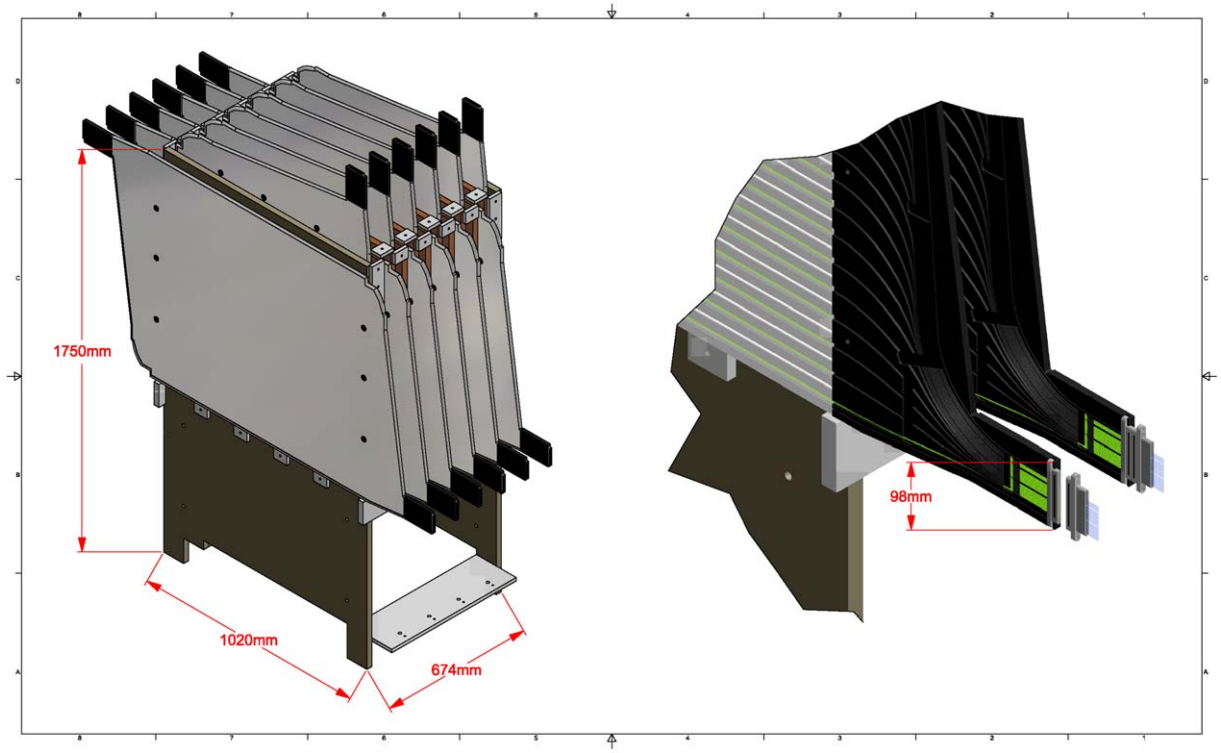

Fig. 1. A CalDet sub-section consisting of 12 planes is shown on the left. The full detector was composed of five such sub-sections to facilitate transportation within the experimental hall. In the figure, the scintillator strips are oriented horizontally in the first plane and alternate between horizontal and vertical orientation in successive planes. Light is carried by wavelength-shifting (WLS) fibers to the snout (shown at right) on each side of the scintillator plane where it is transferred to additional WLS or clear optical fiber and routed to multi-anode phototubes. (Secondary optical fibers and phototubes are not shown).

with the magnetized, 2.54 cm-thick planes used in the Near and Far detectors. The CalDet was composed of five identical sub-sections, with 12 planes in each, allowing relatively easy installation in the test beam areas. The length and type of the readout cables was chosen to mimic the attenuation and therefore light level of the underground detectors. One side of each detector plane was readout using 4 m-long ("green") WLS fiber cables while the other side was readout using 6 m-long clear optical fiber cables. The attenuation difference between the WLS and clear readout also enables a clean-cut demonstration of the detector calibration.

2.2. Readout electronics and data acquisition

The CalDet front-end electronics and readout used to collect the data presented here was identical to the MINOS FD system [11]. When operating with FD electronics, three 16-anode Hamamatsu photomultipliers (PMTs) serviced one side of two successive planes of the same orientation. The readout electronics is based on the multi-channel VA chip produced by IDE Corporation [12]. There is one chip for every phototube, with three chips residing on a VA Front-end Board (VFB) attached to each PMT box. The VFB also houses a pair of photodiodes and an ASDLite [13] which discriminates the common-dynode signal from each PMT at a level of ≈ 0.3 photoelectrons.

Signals input to each VA channel are amplified and shaped with a peaking time of 500 ns. If the ASDLite has triggered, the amplified signals on the VA chip are sampled and held before being output to a 14 bit ADC mounted on a custom VME readout controller (VARC). A single ADC services six VA chips and has a resolution of 2 fC per count. It takes approximately 5–10 μs to digitize the signals from one VA chip. Hence, if the six VA chips serviced by the ADC must all be processed, as is frequently the case in physics events, the last chip will be inactive for up to 60 μs.

Two VME crates, each housing three VARCS, were stationed alongside the detector. The VARCs stored the digitized data in two separate VME memory buffers to permit continuous readout, and performed pedestal subtraction, noise decorrelation, and zero-suppression. An external signal could be fed into the VARC to enable or disable the ASDLite trigger on the dynode pulses. The entire readout system was synchronized by distributing a 10 MHz signal to each VARC. The timing signal was used to generate a 640 MHz clock, thereby allowing the PMTs dynode signals to be time-stamped with a precision of 1.5625 ns. The timing signals were also used to start and stop the runs synchronously and to trigger the VME memory readout.

The CalDet data acquisition system (DAQ) was a scaled down, but otherwise equivalent, version of the MINOS DAQ [14]. Each VME crate contained one single-board VME ReadOut Processor (ROP) [15,16] which provided configuration, monitoring and data input/output. The readout was buffered in the ROP memory and transferred over a PCI Vertical Interconnect (PVIC) [16] interface into the memory of a Branch Readout Processor (BRP) and from there to a Trigger Processor (TP). The TPs ordered the data in time and performed quality monitoring. Output from the TPs was collected, merged, ordered, and written to a ROOT [17] file that was shared with external monitoring and data analysis processes.

3. Test beam layout and data collection

3.1. The PS test beams

The CalDet was exposed in the T11 and T7 test beams in the East Experimental Hall of the 24 GeV/c CERN Proton Synchrotron (PS). The beams are dual polarity, mixed composition (e, μ, π and p), and were operated at momentum settings in the range 0.2–3.6 GeV/c (T11) and 1–10 GeV/c (T7). Both lines were equipped with brass collimators for momentum and intensity definition. Two or three scintillator paddles were placed in the beamline and used to measure the particle time-of-flight (TOF). The two counters were separated by 9.1 m in T7, 12.5 m or 7.3 m in T11, and achieved a resolution of 100–200 ps. Several threshold Cherenkov counters filled with CO_2 were provided to identify electrons at all energies and muons and pions with momenta $\geqslant 1.8$ GeV/c. A schematic of the detectors and particle identification layout is shown in Fig. 2.

3.2. External trigger

The FD electronics was designed to operate in the low-rate environment of the Soudan cavern in which each PMT is independently readout according to its dynode signal. When operated, without alteration, in the relatively high-rate test beam environment, the electronics were dominated by dead-time and pile-up effects. To improve performance, a simple trigger was formed from the coincidence of the two TOF counters. The coincidence signal was transmitted to each VARC and used to enable dynode triggers for ≈ 500 ns. A 60 μs veto was then generated to suppress coincidences while the PMT signals were being digitized. The typical coincidence rate was 1 kHz, a result of balancing the data rate against the effect of pile-up. An additional facility was included in the trigger logic to allow light-injection (LI) and cosmic ray calibration events to be collected between beam extractions.

3.3. Offline event finding

The data acquisition continuously appended newly recorded hits to the set of previously observed hits, flushing the entire record to disk once each second. While collecting beam data, no manipulation (aside from sorting the hits in time order) or online selection was done, so that the data would be as free from bias as possible. The raw data file was processed offline with an algorithm that located events

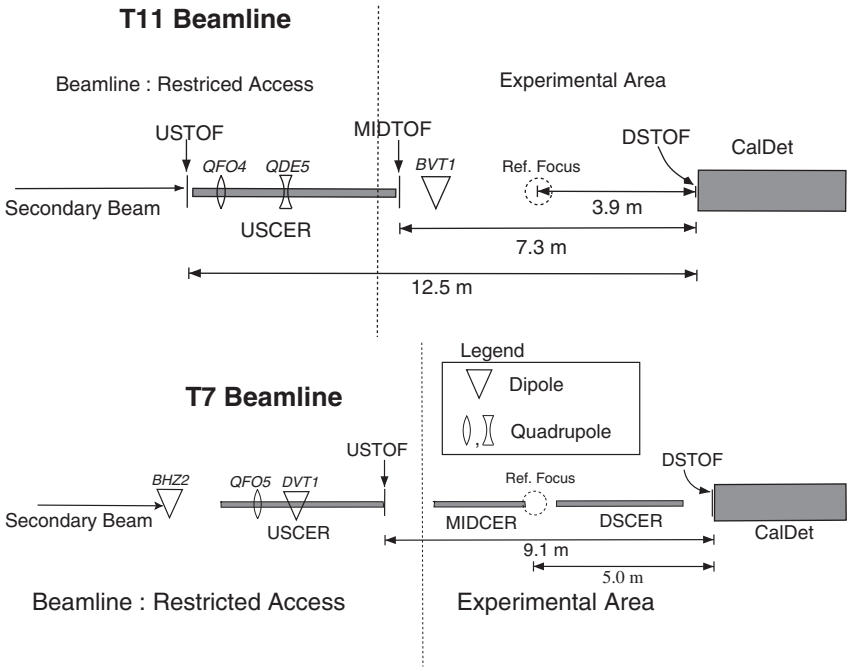

Fig. 2. The test-beam layout showing the detector along with downstream beam elements and particle identification devices. US-, MID-, and DSTOF label time of flight counters. US-, MID- and DSCER label threshold Cherenkov counters.

in the stream of hits and then wrote each event as an individual record in a second file. The algorithm began by searching for clusters of hits separated by time gaps of more than ~156 ns. Each group of hits was then tested for the following trigger conditions:

(1) proximity (within 156 ns) to a coincidence between the beam counters;
(2) proximity to a signal from the Cherenkov counters;
(3) hits in N out of $N+1$ consecutive scintillator planes, with $N = 3, 4, 5$;
(4) proximity to a LI calibration pulse.

Hit clusters that satisfied one of these criteria were flagged with an appropriate trigger word and written to disk. Generally, the first two criteria denoted beam events, while cosmic rays and out-of-spill, accelerator-produced muons were identified with the third criterion.

4. Detector calibration

The principle tools for calibrating the detector were an LED based LI system, cosmic rays, and test-beam muons. The detector was calibrated in a multi-stage procedure that converted the raw signal $Q_{\text{raw}}(i,t)$ measured by channel i at time t into a fully corrected signal Q_{cor}. Each calibration stage produced a numerical factor (“calibration constant”). The fully corrected Q_{cor} was defined as the product of $Q_{\text{raw}}(i,t)$ and the calibration constant from each stage:

$$Q_{\text{cor}} = Q_{\text{raw}}(i,t) \times D(i,t) \times L(i) \times U(i) \times T(t) \times S$$

where D, L, U, T and S refer to

Drift correction $D(i,t)$: LI was used to determine the absolute gain of each channel as well as track the gain over time.

Linearity correction $L(i)$: The LI system was used to linearize the PMT and VA chip response to large signals.

Uniformity correction $U(i)$: Through-going muons were used to account for differences in light output between individual strips and attenuation in the optical fibers.

Temperature correction $T(t)$: The temperature dependent response of the scintillator strips, photomultipliers, and electronics was corrected for.

Signal scale calibration S: The overall scale of the signals was anchored to the detector’s response to stopping muons.

A detailed discussion of the calibration procedure is presented below.

4.1. The light injection system

The calibration procedure was critically reliant upon data collected with the LI system. The system served four purposes:

- It allowed an absolute measurement of each channel’s gain.
- It tracked the gain of each channel over a period long enough to record an adequate number of through-going muons for a complete strip-to-strip response calibration. The tracking was accomplished by injecting light to all strip-ends at regular intervals. These data are known as “drift points”.
- It determined the response of each channel as a function of input charge by injecting light over the range

1–200 photoelectron (PE). These data are known as "linearity curves".
- Finally, the LI system was a powerful monitoring tool that was used to check the integrity of optical connections and electronics channels.

The LI system employed ultra-bright LEDs to inject light into the detector via a series of clear optical fibers which illuminated the WLS fibers by means of a LI module (LIM) mounted on the optical connectors of each plane [18]. The LEDs were driven by a custom-designed pulser box that delivered stable and short electrical signals to the LEDs so that the light pulses were similar to those which would be produced by a charged particle traversing the scintillator. Light from each LED was also transferred, through clear optical fibers, to several PIN diodes. The PINs provided a stable, linear, and independent measurement of the injected light. The light intensity at the PINs was about 1000 times larger than at the PMTs owing to inefficient light transfer in the LIMs and attenuation in the WLS and clear PMT readout cables. The difference was necessary because the PMTs are sensitive to much lower light levels than the PIN diodes.

4.1.1. PMT gain measurement

The gains of the PMTs were calculated using a simple photon counting procedure. Assuming that the initial number of photoelectrons λ at the photocathode is dominated by Poisson statistics then

$$\lambda = \left(\frac{\mu}{\sigma_0}\right)^2, \quad \mu = G\lambda, \quad \sigma_0 = G\sqrt{\lambda}$$

where μ is the mean of the pedestal subtracted ADC distribution and σ_0 is the RMS of the Poisson fluctuations at the photocathode multiplied by the gain G. It is not possible to measure σ_0 directly, instead what is actually measured is the RMS of the ADC distribution, σ_{0m}:

$$\begin{aligned}\sigma_{0m}^2 &= (\sigma_0^2 + \sigma_1^2 + \sigma_2^2 + \cdots + s\sigma_{\text{ped}}^2) \\ &= G^2\left(\lambda + \frac{\lambda}{g_1} + \frac{\lambda}{g_1 g_2} + \cdots\right) + \sigma_{\text{ped}}^2\end{aligned}$$

where σ_i and g_i are the RMS of the photoelectron distribution and the gain at the ith dynode, respectively. Using a similar argument the measured width of the single photoelectron peak, σ_{1m}, is

$$\begin{aligned}\sigma_{1m}^2 &= (\sigma_1^2 + \sigma_2^2 + \cdots + \sigma_{\text{ped}}^2) \\ &= G^2\left(\frac{1}{g_1} + \frac{1}{g_1 g_2} + \cdots\right) + \sigma_{\text{ped}}^2\end{aligned}$$

where $\lambda = 1$ since we are considering the single photoelectron peak. This leads to

$$\lambda = \left(\frac{\mu}{\sigma_{0m}}\right)^2\left(1 + \left(\frac{\sigma_{1m}}{G}\right)^2\right)$$

allowing the light level, λ to be determined. The advantage of this method of photoelectron counting, and therefore gain determination, is that it can be used at high light levels where the pedestal contribution is negligible. Furthermore, it is found to be the most robust method for determining gain, having little dependence on light level.

A simulation of the phototube response was used to test the gain determination method. The simulation assumes that electron multiplication at the ith dynode stage ($i = 1, \ldots, 12$) is a Poisson process with mean $\alpha_i = n_{i-1}g_i$, where n_i denotes the number of electrons present after stage i, n_0 is the number of electrons accepted from the photocathode, and g_i is the secondary emission of stage i. The g_i was defined as $g_i = aV_i^b$ with V_i equal to the voltage drop across stage i and a, b constants chosen to reproduce the evolution of the PMT gain with applied voltage [19]. The gain of the (simulated) PMT is then $G = \prod_i g_i$. One thousand ADC spectra, each with 10 000 entries, were generated at 23 different light levels. The gain was calculated for each spectrum. The means of the resulting gain distributions show no systematic dependence on light level, and vary by less than 0.25% over the range 1–100 PE. The typical error on a single measurement of the gain, inferred from the RMS of the gains measured on the 1000 spectra, is ~1.5%.

The width of the single photoelectron peak, σ_{1m}, is derived by fitting ADC spectra collected at low light levels ($\lesssim$2 PE). The fitting technique, detailed in Ref. [20], assumes a Poisson distribution of photoelectrons from the photocathode and models the nth photoelectron peak as a Gaussian with pedestal subtracted mean, $\mu_n = Gn$, and width, $\sigma_n = \sqrt{n}\sigma_{1m}$. An additional Gaussian term is used to describe photons that pass through the photocathode and produce a photoelectron directly at the first dynode, thereby missing one stage of multiplication. Fig. 3 shows two low light-level spectra with the best fit overlaid. The secondary emission coefficient, approximated from the fit result as $g_1 = (G/\sigma_{1m})^2$, is shown in Fig. 4. The mean of Fig. 4 was used for all of the pixels in the detector, adding a small systematic uncertainty (related to the width of the distribution) to the gain.

4.2. Linearity correction—$L(i)$

The response of the photomultipliers and VA electronics was linearized by illuminating each channel at 24 discrete light levels covering the range 1–200 PE. Response curves were constructed by plotting the charge measured by the PMTs as a function of the charge measured by the PINs. Fig. 5 displays the data points and derived non-linearity curve for a typical channel. Before being used as a calibration the response was scaled to set the slope = 1 in the linear region. Fig. 6 presents the average linearity correction and RMS (shown as bars) for a particular LI linearity run. The RMS increases sharply around 13 000 ADC counts as the response of some channels saturates.

Figs. 5 and 6 show the curves ultimately used to linearize the PMT and electronics response. However, the raw data

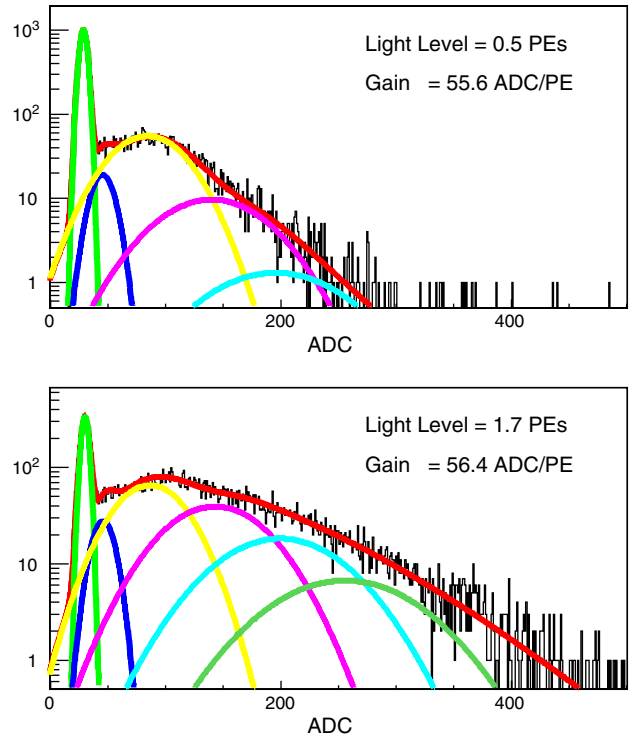

Fig. 3. Two example fits, to the same channel, of the low light level ADC spectrum. The fit consists of Gaussians weighted by Poisson statistics for the pedestal (left-most curve) and first 12 photoelectron peaks (starting with the third curve from he left). An additional term is added to describe the case when a photon passes through the photocathode and produces an electron at the first dynode (second curve from left). The fit is an approximation since the shape of the single photoelectron peak is asymmetric and not ideally described by a Gaussian.

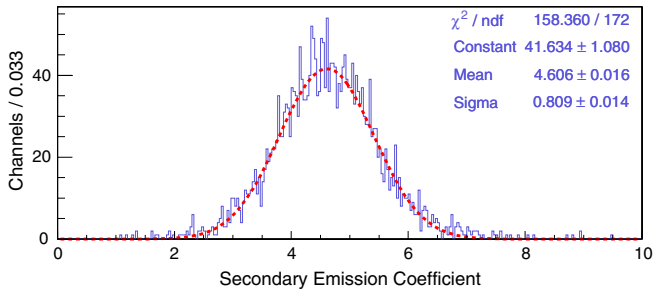

Fig. 4. The secondary emission coefficient (g_1) as calculated from the fits to low light-level ADC spectra.

collected in 2002 displayed a non-linearity for light levels $\lesssim$20 PE, a region where the PMT and electronics had previously been shown to have a linear response. The effect was eventually traced to a small dependence between the voltage applied to the LED and its wavelength spectrum [21], convoluted with a rapidly changing region of the WLS fiber absorption spectrum. This non-linearity is illustrated in Fig. 7, with a straight line fit to the middle portion of the curve.

The low light-level non-linearity was discovered in 2002 during the CalDet beam runs. Subsequently, the three

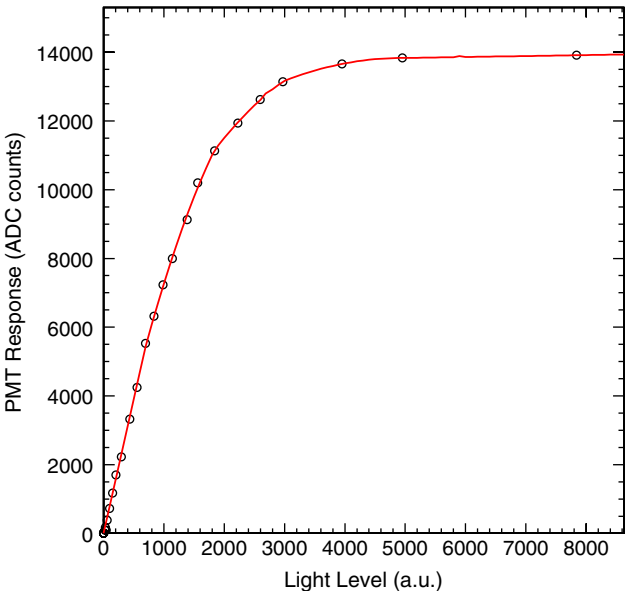

Fig. 5. The response curve for a typical channel. The open circles show the response measured while illuminating the channel with different light levels. The abscissa corresponds to the linear scale described in the text and is proportional to the light intensity. The curve is the derived linearity correction.

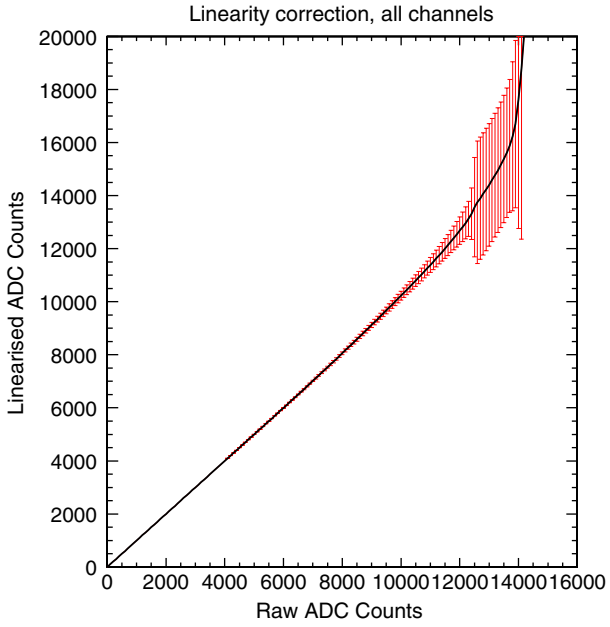

Fig. 6. In black, the average linearity correction as a function of Raw ADC counts. The error bars show the RMS (computed over all channels) of the linearity correction. The sharp increase in RMS at approximately 13 000 ADC counts occurs as the response of individual channels begins to saturate.

MINOS detectors were retrofit with ultra-violet LEDs that do not exhibit this non-linearity. The CalDet data collected in 2002 were corrected for the effect by exploiting the known linearity of the PMTs and VA chips at light levels $\lesssim$100 PE (6000 ADC counts). Each LED illuminated the fibers in several hundred scintillator strips, and each of these strips was readout at the end closest to the LI, the

"near end", and the other end, or "far end". The photomultiplier response curve was mapped out by illuminating the PMTs over a range terminating at 14 000 ADC counts (nearly full-scale) as measured on the near end. Several of the far end channels were selected because they measured less than 6000 ADC counts at the maximum light level. The response of the selected channels was then averaged and used as the linear scale.

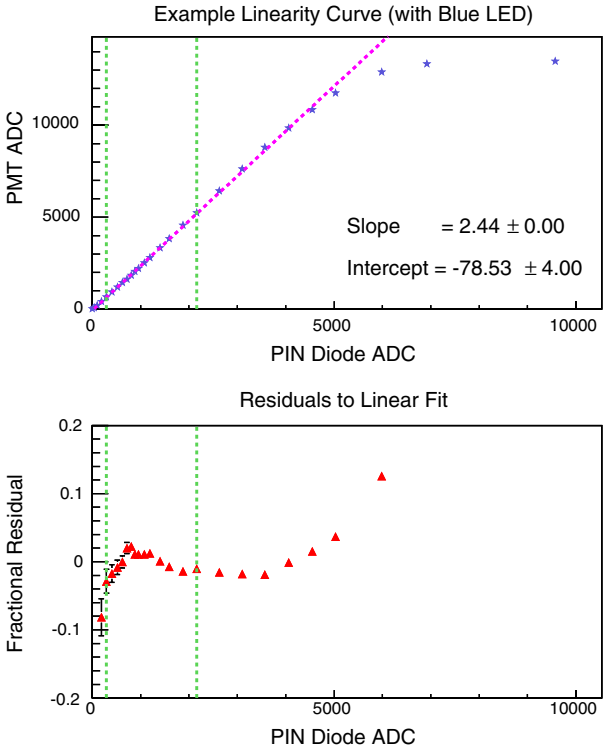

Fig. 7. The upper figure shows the non-linearity in the PMT–PIN response observed when a blue LED was used to illuminate the PMTs through a wavelength shifting fiber. The lower figure presents residuals to a linear fit done within the region marked by the dashed lines. The non-linearity was traced to a slight shift in wavelength emitted with applied voltage on the LEDs, coupled with a rapidly changing section of the wavelength shifting fiber absorption spectrum.

4.3. Gain drift correction—$D(i,t)$

At CalDet, a "drift point" was collected every 20 min by pulsing each channel 2500 times with a ~30 PE signal. The fractional change in response of each channel was then calculated as [20]

$$C(t) = \frac{\mu_{\mathrm{pmt}}(t)/\mu_{\mathrm{pin}}(t)}{\mu_{\mathrm{pmt}}(0)/\mu_{\mathrm{pin}}(0)}.$$

Here $\mu_{\mathrm{pmt}}, \mu_{\mathrm{pin}}$ indicate the means of the PMT and PIN diode distributions, t refers to the time the drift point was taken and $t = 0$ is a fixed reference time. The division by μ_{pin} accounts for (typically small) changes in the LED intensity.

The drift points are used to track changes in the gain of each channel during the period that muons are being collected for the strip to strip equalization discussed in the next section. Fig. 8 shows the drift ($\mu_{\mathrm{pmt}}(0)C(t)$) measured for one channel over a 6-day period. In the FD, due to low muon flux (≈ 500 events/strip/month), it will take more than a month to determine each strip's response with an accuracy of a few percent. The drift correction is necessary because the gain of each channel may drift by several percent during that time. The muon flux is larger at CalDet and a sufficient number of tracks could be collected within about an hour. In practice the strip to strip calibration procedure was only applied once per run period, and the drift point calibration ensured that detector drift over time was removed.

4.4. Correction for strip-to-strip non-uniformity—$U(i)$

Muon tracks are used to correct for strip-to-strip differences in light output and attenuation in optical fibers. The characteristic quantity is defined to be the average

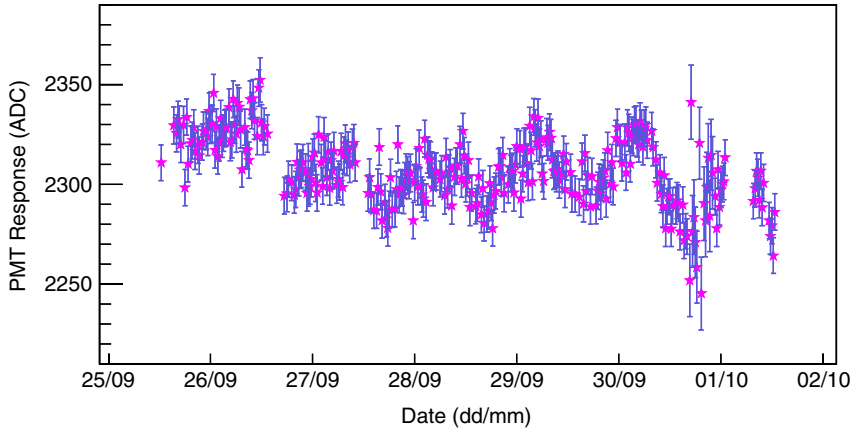

Fig. 8. The response of a single PMT channel measured over the course of 6 days. Each point is the result of a 2500 pulse drift point. The oscillatory shape is due to changes in gain with the ambient temperature.

response to a cosmic ray muon travelling normal to the strip's face and passing through its longitudinal center. Before the equalization can be achieved, corrections must be applied for track angle, path length in the scintillator, the Poisson nature of photoelectron production and attenuation within the WLS fibers. The resulting (corrected) ADC distributions are then compared to a reference strip-end in order to calculate calibration constants of order unity. Application of the $U(i)$ constants produces a calibrated ADC unit that has the same scale for every strip-end.

4.4.1. Correction for track angle and path length

The number of photons produced by a muon passing through a scintillator strip is proportional to the muon's path length within the strip. Therefore, any strip-to-strip differences in the muon path length must be corrected before performing the equalization. For an infinite scintillator plane, the path length Δs would be simply related to the track angle with respect to the z-direction:

$$\Delta s = \frac{\mathrm{d}s}{\mathrm{d}z}\Delta z$$

where the z-axis runs perpendicular to the strip's 4.1 cm face, the y-axis runs along the strip's length, $\mathrm{d}s^2 = \mathrm{d}x^2 + \mathrm{d}y^2 + \mathrm{d}z^2$, and $\Delta z = 1$ cm is the thickness of the scintillator plane.

For finite strips, the path length through any single strip may be smaller than the value above since muons can traverse more than one strip in a plane ("corner clipping") as illustrated in Fig. 9. Corner clipping is particularly important in the CalDet because the strips are oriented either horizontally or vertically [1] and the angular distribution of cosmic rays is isotropic in the horizontal plane but peaked at the zenith in the vertical. This leads to significantly different path lengths in the horizontally and vertically oriented strips.

The MINOS detectors do not have sufficient spatial resolution to measure the true path length through each strip. Instead, an average path length is calculated based on the track angles and the dimensions of the scintillator strip. Using purely geometrical considerations, the average path length for a fixed angle $\theta = \arcsin(\mathrm{d}y/\mathrm{d}s)$ can be calculated. Assuming that the muon entry point across the transverse width of the strip, y, is a uniform distribution, the average path length is obtained by integrating over all possible entry positions:

$$\langle \mathrm{d}s \rangle = \frac{\int_0^{\Delta y+\delta y} \mathrm{d}s(y)\,\mathrm{d}y}{\int_0^{\Delta y+\delta y} \mathrm{d}y} = \frac{\mathrm{d}s}{\mathrm{d}z}\Delta z\left(\frac{\Delta y}{\Delta y + \Delta z|\mathrm{d}y/\mathrm{d}z|}\right).$$

[1] Strips are oriented ±45° to the vertical in the underground detectors.

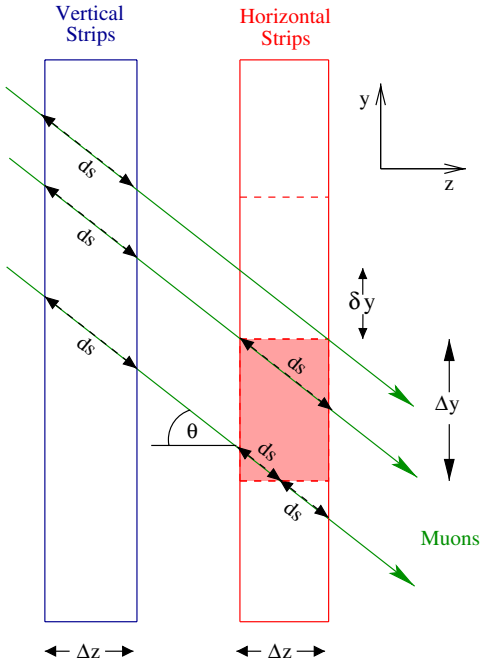

Fig. 9. A sketch showing how the average path length varies between the horizontal and vertical strips. The average path length in the horizontal strips is smaller as there is a larger chance that the muon will traverse two or more scintillator strips in one plane. In the MINOS detectors the plane thickness $\Delta z = 1$ cm and the transverse strip width $\Delta y = 4.1$ cm.

Here $\Delta y + \delta y$ is the maximum y position for which the muon will still pass through the strip, $\Delta y = 4.1$ cm is the transverse strip width, and $\mathrm{d}y/\mathrm{d}z = \tan\theta$.

This average path length can then be used to correct each hit along a track and account for the differing path length distribution in the horizontal and vertical strip orientations. However, as shown in Fig. 10, even after applying this correction, a ~5% discrepancy between horizontal and vertical strips is still observed. The primary contribution to the remaining discrepancy arises from cases in which, although a muon has passed through the strip, no photoelectrons were created. This effect is considered in the next section.

4.4.2. Correction for photoelectron statistics

The mean pulse-height observed for normally incident muons passing through the center of each strip is ≈ 3.8 PE per strip-end. Therefore, based on Poisson photoelectron statistics, approximately 2% of muon crossings are expected to produce no photoelectrons. Tracks that clip the corner of a strip are even more likely to produce zero PEs, causing the magnitude of the effect to differ between the horizontal and vertical strip orientations. The calibration procedure must account for the possibility of observing no signal; otherwise the mean of the signal distribution is a biased estimator of the light output which makes it impossible to completely remove the variations in light output.

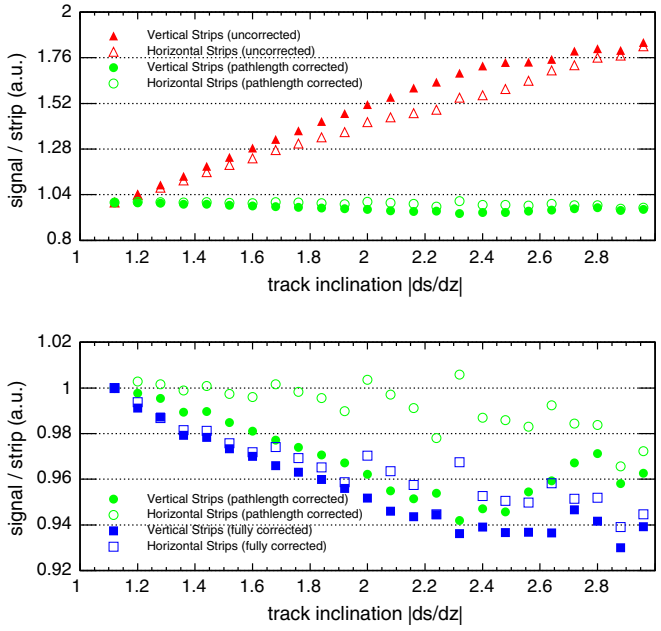

Fig. 10. The upper figure shows the mean signal from cosmic ray muons, as a function of the track inclination ds/dz , for the horizontally and vertically oriented strips before and after application of the path-length correction. The ordinate is scaled to the mean signal at $ds/dz = 1$. The bottom plot is a close-up of the response, showing a ~5% difference between the horizontal and vertical strips when only the pathlength correction is applied.

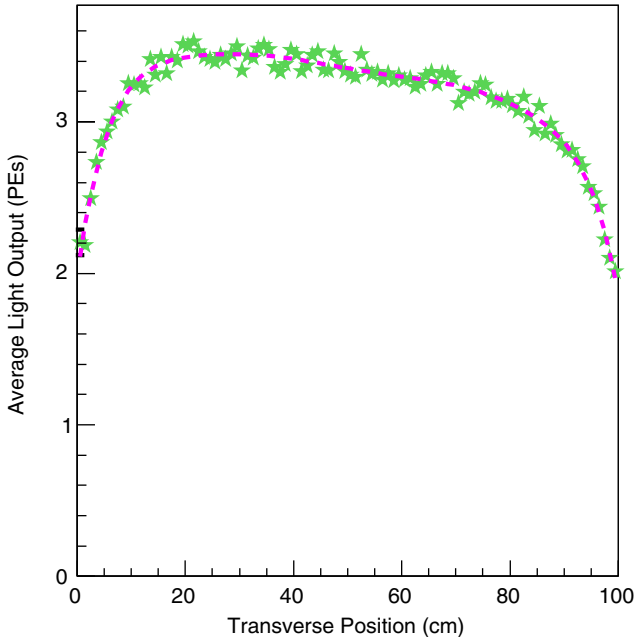

Fig. 11. Muon light output as a function of position along the strip, shown for the WLS fiber readout of horizontally oriented strips. The decrease in light output at the edges of the strips is due to a lack of reflective coating which allowed light to escape prior to absorption in the wavelength shifting fiber.

The average probability of observing no signal, $\langle P_0 \rangle$, for a fixed angle is given by

$$\langle P_0 \rangle = \frac{\int_0^{\Delta y+\delta y} e^{-\lambda ds(y)} dy}{\int_0^{\Delta y+\delta y} dy} = \frac{e^{-\lambda(ds/dz)\Delta z}(\Delta y - |dy/dz|\Delta z) + 2|dy/dz|/\lambda(ds/dz)(1 - e^{-\lambda(ds/dz)\Delta z})}{\Delta y + |dy/dz|\Delta z}$$

where λ is the mean number of photoelectrons obtained from a muon passing through 1 cm of scintillator. For each hit used to form the muon ADC spectrum, the ADC value is weighted by the probability of observing a signal: $1 - \langle P_0 \rangle$, and the zero bin is weighted by the probability of observing no signal: $\langle P_0 \rangle$. The mean of the resulting ADC distribution is used to estimate the light output.

Since λ is not known a priori, the correction procedure is iterative and the gain of the PMTs and electronics must have already been determined. The method is also extended to account for the single photoelectron hits that fall below the pedestal suppression threshold. Fig. 10 shows the response to cosmic ray muons after the correction procedure was applied. Although there is still a residual dependence of the muon response on the track angle, the asymmetry between the two strip orientations is significantly reduced, particularly in the region $ds/dz < 2$ in which 80% of muon tracks occur. The residual dependence on the track angle introduces a small offset into the calibration constant that depends on the angular distribution of the muon tracks used in the calibration. That offset is removed by the response scale calibration of Section 4.6.

4.4.3. Attenuation correction

Fig. 11 shows the average signal created by normally incident muons as a function of position along the strip.[2] The distribution is not purely exponential due to substantial leakage of light through the (unreflective) strip-ends. Although the overall attenuation for the strip-ends readout with WLS fiber is larger than for the strip-ends readout with clear fiber, there is a shallower attenuation curve in the center of the scintillator layer which reflects the fact that the WLS fiber has both long and short attenuation components. For attenuation correction purposes, the four distributions of Fig. 11 are made for the 24 strips in each plane in order to account for small systematic differences in the lengths of the WLS fibers. The distributions are parameterized with a high-order polynomial and are used to remove the effect of the attenuation from cosmic ray muons, establishing the calibration constants at the longitudinal center of each strip (= 50 cm in Fig. 11).

4.5. Correction for temperature variations—$T(t)$

The manner in which the detector's response depends upon temperature variations was studied using cosmic ray

[2]The distribution is the average over all horizontally oriented strips readout through WLS fibers. Similar distributions are obtained for the vertical strips and the clear-fiber readout.

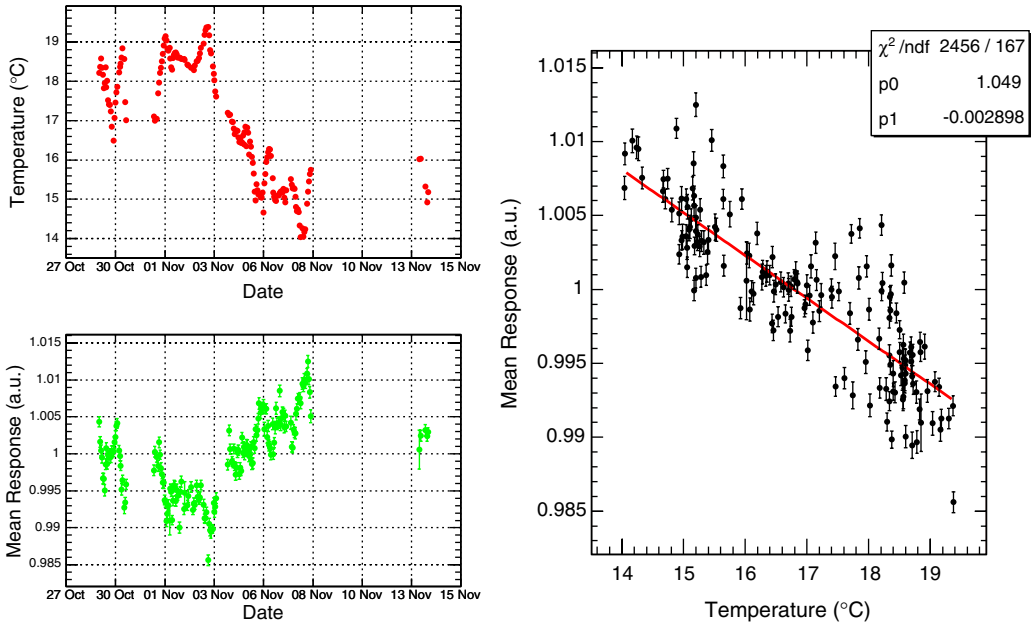

Fig. 12. The top left-hand figure shows the average air temperature for each of the runs used in the study. The bottom left-hand figure shows the change in the response (to cosmic ray muons) as a function of time. The right-hand figure shows the response as a function of air temperature, along with a straight line fit used to characterize the dependence.

muon samples obtained when the CalDet was situated in an enclosure in the PS East Area hall. The PS was off when the data were collected so only cosmic ray muons were present. The temperature was recorded at 1-min intervals with a commercially available temperature probe. $U(i)$ calibration constants were calculated hourly using the prescription described above.

The measurements demonstrated that the response of the detector depends on its temperature. The dependence is known to have two distinct contributions. First, bench tests have demonstrated that the gain of the electronics exhibits a temperature dependence $\sim -0.22\,\%/^{\circ}\mathrm{C}$. This is not accounted for by the LI calibration because the PIN diodes are readout by the same electronics as the PMTs. After correcting for the electronics, the remaining temperature dependence is attributed to the scintillator light output. Fig. 12 shows the response (without electronics correction) to cosmic ray muons as a function of ambient air temperature. A linear fit is used to characterize the (total) dependence as $\sim -0.30\,\%/^{\circ}\mathrm{C}$ of which $\sim -0.08\,\%/^{\circ}\mathrm{C}$ is attributed to the scintillator. These results are applied to correct the data to a reference temperature of 18 °C.

4.6. Signal-scale calibration—S

The CalDet was decabled in order to move it to and from the test beam enclosures. The decabling and recabling modified optical and electrical connections in the detector and, without an additional calibration to anchor the scale of observed signals, rendered the data collected in different runs incomparable. Moreover, a signal-scale calibration was needed to translate the measurements made by CalDet to the Near and Far detectors. At CalDet, the response to beam muons, collected at momentum settings of 1.4–2.0 GeV/c, was used to fix the pulse-height scale, thereby providing the calibration. These muons range out in the detector and therefore the muon momentum may be estimated for any point along the track, based on the distance between the point and the end of the track. The similarity in construction of the MINOS detectors means that the calibration may be carried to the Near and Far detectors by measuring their response to stopping (cosmic ray) muons.

The simplest way to characterize the detectors' response to muons would be to sum the signal from each hit along the muon track. In practice a sum is not adequate because energy-loss straggling causes the muon range distribution to be spread over several detector planes (≈ 4 planes for a 2 GeV/c μ). The result is that the number of scintillator hits included near the end of the track fluctuates. These hits are particularly problematic because they are created by the muon at low momentum ($\lesssim$400 MeV/c), where the $\mathrm{d}E/\mathrm{d}x$ is a rapidly changing function of $\beta\gamma$. The summed signal, and even the signal per hit, are dependent on the underlying muon momentum in a fashion that is not linearly related to the track length.

Instead of using the summed signal, a more robust technique was developed. The technique measures the response of muons only where their momentum is in the range 0.5–1.1 GeV/c (known as the "track-window"), discarding the portion of the muon track where the energy is between 0.0 and 0.5 GeV/c. By selecting the track section in this way, the rapid increase in ionization at the end of the track is avoided, as shown in Fig. 13. Since the $\mathrm{d}E/\mathrm{d}x$ is

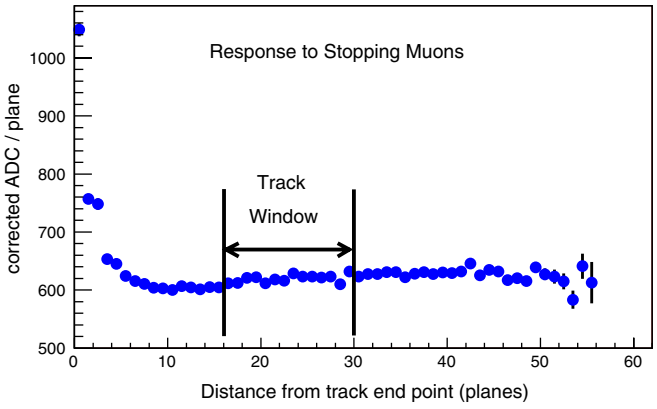

Fig. 13. The average response to stopping muons as a function of the distance from the end of the track along with the window used in the signal-scale calibration. The signals were corrected for gain drift, non-linearity, strip light-output non-uniformity and temperature fluctuations.

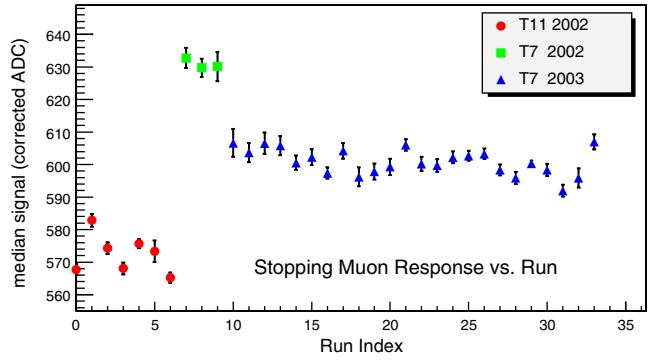

Fig. 14. The median signal observed in the track window for stopping muons in three different data-taking periods. The signals used have been corrected for gain drift, non-linearity, strip non-uniformity and temperature fluctuations. The calibration constant S is defined as the inverse of the median signal. The difference between data-taking periods is a consequence of partially dismantling the detector to move it into the test beam enclosure. During the dismantling and subsequent reconstruction the effective light output changed, probably due to differences in attenuation within optical connections.

relatively constant in the 0.5–1.1 GeV/c region, a 2% error on the muon stopping position translates into an approximate 0.1% error in the energy deposition.

The beam muons used in the calibration were identified as events with a single track entering the detector within the transverse region covered by the downstream trigger paddle and penetrating more than 31 planes. The events were additionally required to have TOF and Cherenkov - measurements consistent with a muon at the nominal beam momentum. Stopping muons were selected by requiring the track to terminate more than two planes from the downstream end of the detector and less than 12 cm from the detector's edge in the horizontal and vertical planes. A final cut on the path length was used to remove tracks more than 20% shorter or 15% longer than expected for a muon with the nominal beam momentum [22].

Fig. 14 shows the median signal observed in the muon track-window for several runs in three separate data-taking periods. The signals were previously corrected for gain drift, non-linearity, strip non-uniformity and temperature fluctuations. The 10% difference in response between T11 and T7 in 2002, caused by breaking and remaking optical connections, exemplifies the need for the signal-scale calibration. The calibration constant S is defined as the inverse of the median signal and a single constant is calculated for each data-taking period by averaging over runs. After application of the entire calibration procedure the fully corrected signals Q_{cor} are said to be in muon equivalent units (MEU[3]). When expressed in MEU, the measured response to hadrons and electrons may be transferred between the T11 and T7 beamlines and to the Near and Far detectors.

5. Validation of the calibration chain

5.1. Validation of the gain drift correction

Fig. 15 demonstrates the efficacy of the drift correction. The figure was constructed by measuring the detector's response to 1 GeV/c electrons before and after applying a 25 V decrease to the PMT high voltages. The high voltage change introduced a 26% decrease in the PMT gains. LI drift points were used to correct the signals from each phototube, after which the detector response in the two runs agreed to better than 0.5%. Typical gain variations were more than 10 times smaller than the one introduced in this test.

5.2. Validation of the uniformity calibration I

The energy deposited by stopping muons varies smoothly and almost linearly over a large fraction of the muon's range within the detector. The stopping muon sample can therefore be used to test the detector's calibration at the strip level by fitting the slowly varying region of the $\mathrm{d}E/\mathrm{d}x$ curve and tabulating the deviations from the best fit at each plane. Fig. 16 shows the results of this procedure when 1.8 GeV/c beam muons (which stop at around plane 50) were used. The signal observed per scintillator plane is shown in the upper figure with and without the application of the calibration constants. A histogram of the residuals from a straight line fit to the first 38 planes are shown in the lower figure. Uncalibrated, the width of the residual distribution is approximately 15%. With calibration, the width reflects the performance of the strip-to-strip equalization procedure and shows that the scintillator planes are calibrated with an accuracy $\approx 1.6\%$.[4] The residuals corresponding to planes with horizontal and

[3]One MEU corresponds to a signal approximately 5% larger than that expected for a minimum ionizing particle (MIP).

[4]The muon beam irradiates approximately two of the 24 strips in each plane. Therefore, the accuracy of the calibration of each strip is approximately $\sqrt{2} \times 1.6\% = 2.3\%$.

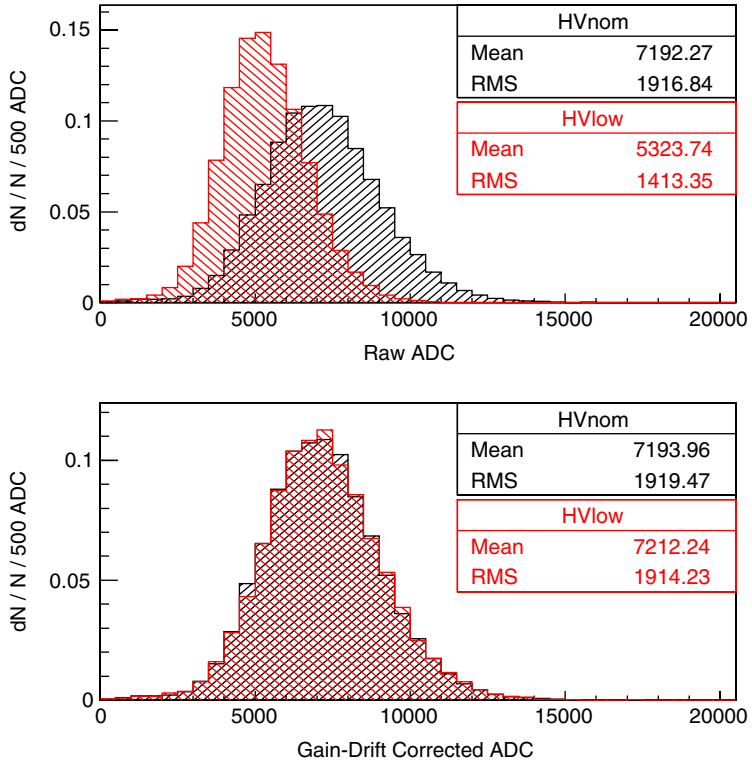

Fig. 15. The upper figure shows the summed signal, in uncalibrated ADC counts, measured for 1 GeV/c electrons. Two runs were taken, one with the PMT high voltages at their nominal values and the other after decreasing the high voltage of each PMT by 25 V. The lower figure shows the summed signal after the gain drift correction ($D(i,t)$) was applied. The correction was able to reduce a 26% discrepancy to less than 0.5%.

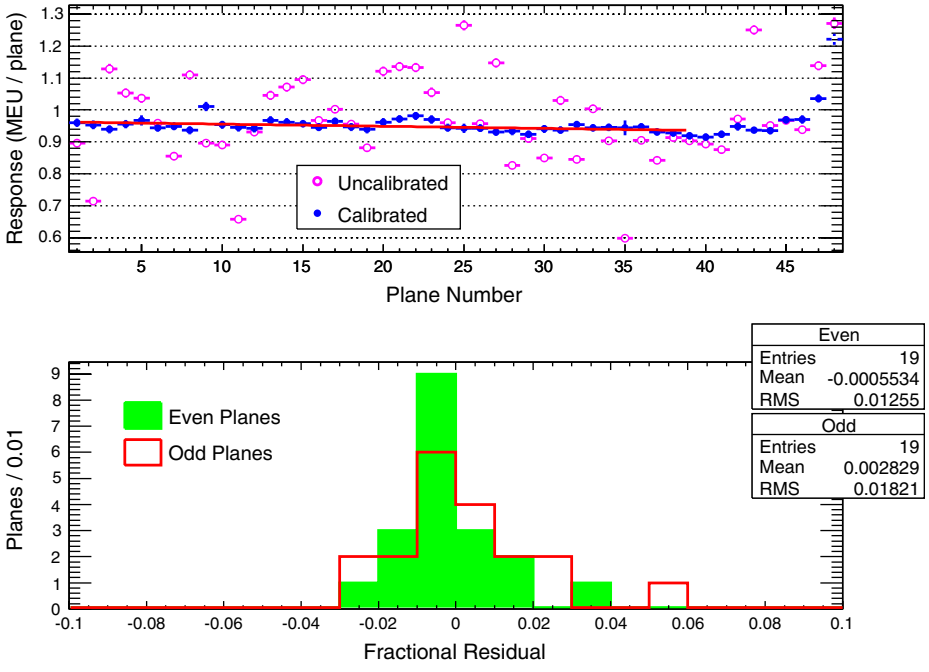

Fig. 16. The performance of the strip-to-strip equalization procedure. The upper figure displays the average signal per scintillator plane measured with a sample of 1.8 GeV/c stopping beam muons. The measurements are shown before and after the application of the uniformity calibration ($U(i)$). A linear fit was done to the calibrated points and the residuals were used to fill the histograms in the lower figure. The RMS of the residual distributions indicates the planes were calibrated with an accuracy of $\approx 1.6\%$.

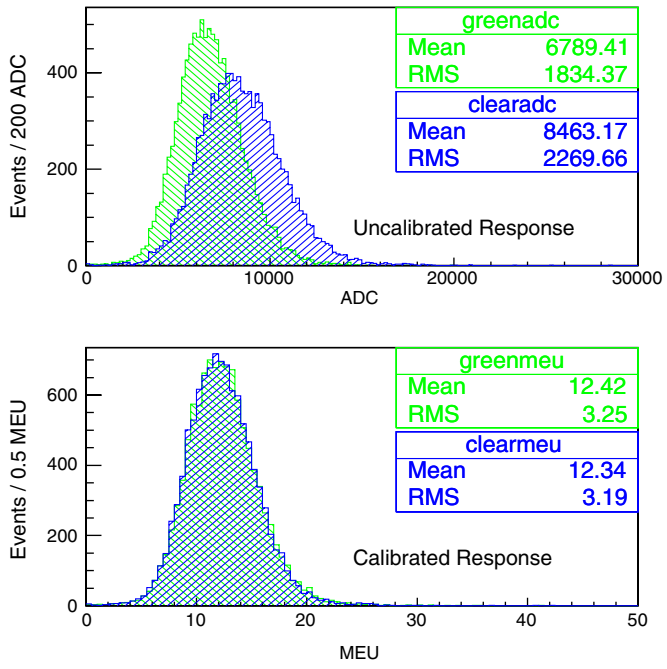

Fig. 17. The response of 1 GeV/c electrons when measured through WLS fibers as compared to measured through clear fibers. The top plot shows the response before application of the uniformity calibration constants ($U(i)$) while the bottom shows the calibrated response. Before calibration the response at each end differs by ~20%, after calibration, the means agree to better than 1%.

vertical strip orientations (even and odd numbered planes, respectively) are histogrammed separately and both distributions have means consistent with zero.

5.3. Validation of the uniformity calibration II

The light level on the sides of the detector readout by WLS fibers is about 25% lower than on the sides readout by clear optical fibers. The strip-to-strip calibration is intended to remove such differences, equalizing the response observed on each side. Fig. 17 validates the calibration by comparing the uncalibrated and calibrated response to 1 GeV/c electrons for the clear and WLS readout. After calibration, the response agrees to better than 1%.

5.4. Validation of the combined calibration procedure

Another powerful cross check of the calibration exploits the expected linearity of the electron response as a function of incident electron momentum, and the independence of the response in the two beamlines. That is, the calibration can be constrained by studying the electron response at several momentum settings in both beamlines. If the detector (and both beamlines) are perfectly calibrated then the measured points should all lie upon the same curve.

Before the electron response in the two beam lines can be compared, the energy loss of particles in the upstream beam elements and PID detectors must be taken into account. In order to estimate the extent of this energy loss, the material upstream of the detector in each of the beam lines was modelled using GEANT3. By comparing the simulated response of the CalDet to particles that travel through the upstream material to the simulated response of particles that do not, the effect of any energy loss upstream of the detector can be estimated. At the 200 MeV/c beam setting the energy loss is a 12% effect but rapidly decreases with momentum, reaching ~3% by 1 GeV/c.

After correction for energy loss the combined T11 and T7 data set are fit with a straight line. The residuals are indicative of a combination of the quality of the calibration, the linearity of the electron response, the accuracy of the beam momentum settings and efficacy of the energy loss correction. Fig. 18 shows the results of the fit. The RMS of the residual distribution indicates that the calibration has an accuracy of at least 1%. The calibration may actually be better than the RMS suggests since the residuals display a systematic dependence on the beam momentum for settings larger than 4 GeV/c. The dependence is possibly due to small differences in the calibration of the beamlines themselves.

5.5. Absolute muon energy calibration

The relatively fine segmentation of the MINOS detectors allows the energy deposited by a muon to be measured as a function of the amount of material traversed by that muon. For those muons that stop in the detector the mean momentum at any point along the muon track may be calculated by integrating the Bethe–Bloch equation from the stopping position to the point in question. The integration yields the mean energy lost in each scintillator plane which may then be compared to the average signal recorded by the detector. This principle was used to fit the Bethe–Bloch equation to data collected by the CalDet, thereby determining the constant relating measured signal and muon energy loss. The fits also served as an additional consistency check of both the uniformity correction $U(i)$ and the stopping muon sample itself.

For every stopping muon event the signal measured in each plane was corrected for the local track angle and histogrammed as a function of the distance (in planes) from the stopping position. The gain drift, light-output non-uniformity, linearity and temperature calibrations were applied to the signals. The mean of the signal distribution in each of the planes was then used in a fit to the Bethe–Bloch equation. The fitting procedure divided each steel plate and scintillator plane into 300 and 30 slices, respectively. For each slice the muon momentum was held fixed while the energy loss was calculated. The momentum was then updated to account for that loss before calculating for the following slice. The fit began by working backward (i.e. calculating the energy gained) from the downstream end of the stopping scintillator plane, starting with a momentum, p_{last}, that was included as a free

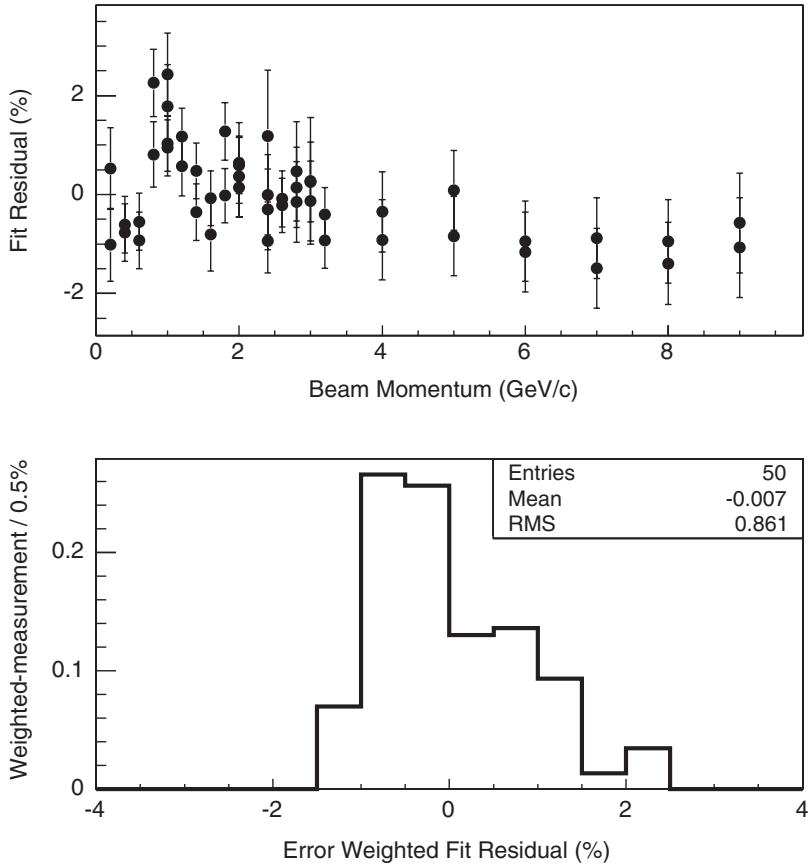

Fig. 18. The upper figure shows the residuals from a linear fit to the electron response as a function of beam momentum. The residuals were weighted by their relative errors and histogrammed in the lower figure.

parameter in the fit. The p_{last} parameter is expected to take a value less than the momentum above which a muon will penetrate a 2.5 cm steel plate ($\approx 120\,\text{MeV}/c$ [23,24]). A χ^2 was then calculated using the mean signal in each plane m_i, the uncertainty σ_i and the expected energy loss ΔE_i:

$$\chi^2 = \sum_i \frac{(m_i - C\Delta E_i)^2}{\sigma_i^2}.$$

The uncertainty includes the statistical uncertainty summed in quadrature with a calibration uncertainty of $1\%/\sqrt{4}$. The numerator is an estimate of the calibration error in each plane. The denominator accounts for fluctuations in the track range which cause each bin in Fig. 19 to receive contributions from approximately four planes. The constant C is a parameter converting the energy lost into measured signal. ROOT's MINUIT derived fitter was used to vary C and p_{last} until the fit converged. Fig. 19 shows one such fit. The data from individual runs were fit independently and the results were combined for each running period. A summary of the fits is presented in Table 1. The variance in the parameter C reflects differences in the absolute light level, electronics and phototube gains caused by recommissioning the detector for each running period. By combining C with the scale constant S determined with the track-window technique of Section 4.6 we find that one

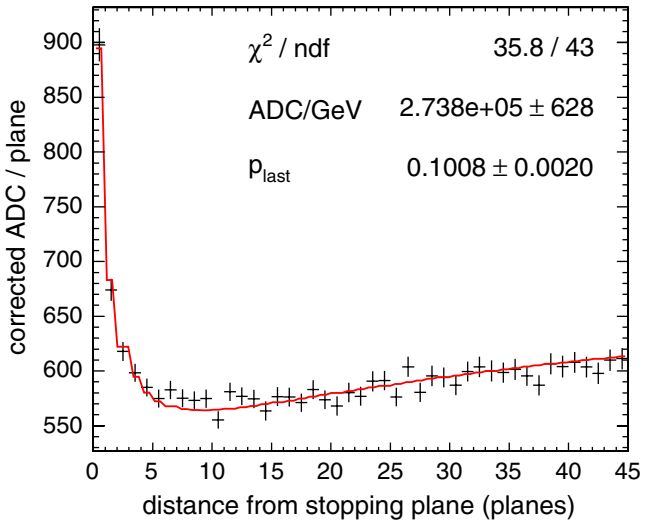

Fig. 19. The Bethe–Bloch equation fit to muon energy loss data collected by the CalDet. The mean of the measured signal distribution in a plane is displayed as function of the distance from the end of the muon track. The data are shown as crosses and the fit as a line. The fit parameter ADC/GeV establishes the relationship between the measured signal and the energy lost by muons in the CalDet scintillator.

MEU corresponds to 2.00 ± 0.01 MeV of muon energy loss in scintillator. The uncertainty is determined from the spread among the three running periods.

Table 1
Bethe–Bloch fit results

Period	T1102	T702	T703
C (ADC/MeV)	287.7	312.3	298.6
MeV/MEU	1.99	2.01	2.00

The ADC values have been corrected for gain drift, non-linearity, light-output non-uniformity and temperature fluctuations.

6. Summary

The MINOS Calibration Detector has been used to develop and demonstrate the calibration procedure to be used at both the large MINOS detectors. The procedure corrects for gain non-uniformity, gain drift over time, PMT and electronics non-linearity, non-uniformity in strip light output, attenuation in optical cabling, and temperature dependent response variations. Furthermore, a portable muon energy unit (MEU) has been established so measurements made at CalDet may be transported to the underground detectors. The large amount of data collected in the T11 and T7 test beams at CERN was used to verify that the calibration procedure can remove systematic effects to a level of 2% or better.

Acknowledgements

The MINOS collaboration would like to thank the UK Particle Physics and Astronomy Research Council and the US Department of Energy for funding this research, and CERN for providing the test beams and support. Special thanks are due to L. Durieu and M. Hauschild for their help throughout this project. We would also like to thank J. Alner, B. Choudhary, H. Kim, A. Lebedev, N. Felt, J. Oliver, P. Sullivan, B. Rebel, J. Musser, P. Smith, M. Marshak and N. Longley for their help in constructing the calibration detector as well as C. Howcroft, M. Thompson, N. West and R. Hatcher for computing and data acquisition assistance. We appreciate the steady interest and advice of S. G. Wojcicki. We are grateful for the engineering support provided by T. Durkin, M. Proga, D. Atree, J. Trevor, J. Hanson, M. Williams, P. Groves and G. Sillman. M. Proga also deserves our thanks for preparing Fig. 1. This work was supported in part by DOE Grant DE-FG03-93ER40757.

References

[1] E. Ables, et al., P-875: a long baseline neutrino oscillation experiment at fermilabFERMILAB-PROPOSAL-0875, 1995.
[2] The MINOS Collaboration, The MINOS Detectors Technical Design Report, NuMI-L-337, 1998.
[3] K. Anderson, et al., The NuMI Technical Design Report (Fermi National Accelerator Laboratory), December 2002.
[4] Y. Ashie, et al., Phys. Rev. Lett. 93 (2004) 101801.
[5] M.H. Ahn, et al., Phys. Rev. Lett. 90 (2003) 041801.
[6] M. Apollonio, et al., Eur. Phys. J. C 27 (2003) 331.
[7] The photomultipliers were sixteen-anode Hamamatsu R5900-00-M16 taken from the same production run as the photomultipliers used for the Far Detector.
[8] A. Pla-Dalmau, Extruded plastic scintillator for the minos calorimeters, in: Annecy 2000, Calorimetry in high energy physics 513–522.
[9] The WLS fibers are a J-type, Y11, multi-clad PMMA, non-S, made by Kuraray, and doped with 175 ppm K27 dye which has maximum intensity emission at 520 nm. The light attenuation in the WLS fibers is well modeled by a double exponential fall off with $\lambda_1 \approx 0.7$ m and $\lambda_2 \approx 3.9$ m. The clear fibers were also manufactured by Kuraray and have an attenuation length $\lambda \approx 13$ m.
[10] Shell EPON 815C epoxy was used.
[11] J. Oliver, N. Felt, G. Feldman, A. Lebedev, R. Lee, IEEE Trans. Nucl. Sci. NS-51 (2004) 2193.
[12] Ideas ASA, Veritasveien 9, Box 315, N-1323 Høvik, Norway.
[13] A description of the ASDLite can be found at <http://bmc.bu.edu/bmc/lerb2/paper_html/paper_html.html> and <http://heplsrv1.harvard.edu/~minos/minos-elec/UsersManVer1.00.pdf>
[14] A. Belias, et al., IEEE Trans. Nucl. Sci. NS-51 (2004) 451.
[15] The ROPs were Creative Electronics Systems RIO3 single board computers running VxWorks on a 400 MHz PowerPC CPU with 64 MB memory.
[16] Creative Electronics Systems, a.A, 39, Avenue vEugene-Lance, CH1212, Petit-Lancy, Switzerland <http://www.ces.ch/>
[17] R. Brun, F. Rademakers, Nucl. Instr. and Meth. A389 (1997) 81.
[18] P. Adamson, et al., Nucl. Instr. and Meth. A492 (2002) 325.
[19] S.-O. Flyckt, C. Marmonier (Eds.), Photomultiplier Tubes—Principles and Applications, Photonis Imaging Sensors, 2002.
[20] R. Nichol, Calibration of the MINOS Detectors, Ph.D. Thesis, University College London, FERMILAB-THESIS-2003-41, 2002.
[21] P. Adamson, et al., Nucl. Instr. and Meth. A 521 (2004) 361.
[22] J.J. Hartnell, Measurement of the Calorimetric Energy Scale in MINOS, Ph.D. Thesis, St. John's College, Oxford, 2005.
[23] D.E. Groom, N.V. Mokhov, S.I. Striganov, At. Data Nucl. Data Tables 78 (2001) 183.
[24] A minimum ionizing muon loses about 28.5 MeV/c per 2.5 cm steel plate. However, at the end of the track the energy loss climbs up the Bragg peak and the stopping power becomes much larger.